CIS-TR-86-04

Artifacts at the Limit of Resolution

Kent A. Stevens
Daniel P. Lulich

Department of Computer and Information Science
University of Oregon

Artifacts at the Limit of Resolution

KENT A. STEVENS AND DANIEL P. LULICH

Abstract **— A visual illusion which appears at the limit of resolution is used to investigate perceived artifacts of the convolution by Gaussian filters. Evidence is provided that implicate the smallest size operator at the retina and that suggest that the perceived shape of intensity changes is influenced by artifacts induced by the operator.**

Index Terms **— Visual resolution, Gaussian filters, zero crossings, edge detection.**

I. INTRODUCTION

A proposed method for detecting edge-position in an image is the marking of zero-crossing contours in the convolution of the image with, e.g., the Laplacian of a Gaussian ($\nabla^2 G$) operator or the similar Difference of Gaussians (DOG) operator [5, 6, 7]. There is evidence that a similar method is involved in human vision, suggested in part by the modelling of the retinal ganglion X-cell as a DOG [2, 5, 9, 10]. Recently, Torre and Poggio [7] have suggested several psychophysical experiments which bear on the shape of the operator. We describe here an illusion that arises at the limit of visual resolution, that implicates the smallest size operator at the retina and suggests that the perceived shape of intensity changes are influenced by artifacts from a DOG operator.

II. BACKGROUND: THE ILLUSION

The illusion is generated by a black and white checkerboard embedded in a background grey, where the grey is chosen to match the spatially-averaged brightness of the checkerboard. The present study was prompted by an earlier observation that the squares along the margin of a checkerboard viewed at a sufficiently small scale seemed distorted — larger and slightly elongated compared to the squares found in the interior of the checkerboard particularly when the checkerboard was embedded in a background grey. The illusion was particularly

interesting when viewed from a distance such that the interior squares were just resolved. Those squares along the margin of the checkerboard persisted so that the checkerboard became only an outline defined by the just-resolvable black and white blobs (minute, slightly elongated pinpoints) while on either side of the margin only a uniform grey was apparent. It was a straightforward matter to convolve the pattern with a range of DOGs of different scales to see if the effect could be attributed to artifacts of the early visual processing of the intensity pattern. The results, shown below, are consistent with the impression of distorted shape one sees in the pattern, and are quantitatively predicted when one scales the checkerboard pattern according to the expected smallest size of DOG operator in human vision. At the time the illusion seemed to suggest that if the shape of minute intensity changes were demarked by zero-crossings, that the zero crossing loci are represented with a granularity finer that one arc minute. That is, if the apparent distortions in the shapes arise from artifacts in the zero-crossing loci, one might conclude that the zero-crossings are explicitly represented with resolution roughly within the hyperacuity range [T. Poggio, personal communication, 1978]. The checkerboard pattern seems to suggest explicit interpolation in the hyperacuity range, consistent with that conventionally found by forced-choice experiments [8]. However, the mere fact that the zero-crossings in the convolved checkerboard pattern seemingly resemble the shapes one sees in the pattern does not necessarily implicate zero-crossings as being the representational primitive. R. Watt pointed out that alternative schemes to zero crossings, such as the "zero valued stationary point" would exhibit similar artifacts [personal communication, 1982].

Since that initial study of the checkerboard artifacts, other researchers have provided a computational framework for describing the artifacts [1, 7]. Berzins [1] has shown that the zero-crossings of $\nabla^2 G$ operators are subject to a variety of inaccuracies in following the true

position of an edge. When analyzing a square in an image, if the length of an edge of the square is greater than the space constant σ of the $\nabla^2 G$ then zero-crossing displacements are dominated by errors of the Laplacian approximation to the directional derivative. On the other hand, as the length of an edge becomes smaller than σ, displacements are due to the smoothing properties of the underlying Gaussian. As the length of an edge approaches zero with an operator of σ equal to one, the contours approach a circle with the radius $\sqrt{2}$ standard deviations. The deflection of the zero-crossing locus are said to "swing wide" of the corner.

III. Gaussian Artifacts

If the human visual system performs a similar computation utilizing *DOG* operators, then when presented with a square smaller than σ of the smallest size *DOG* operator, the local convolution of the intensity image should be subject to swing-wide artifacts. If the encoded version of the convolution is available for later perceptual interpretation then subjects should report seeing the artifacts. Our checkerboard patterns appear to elicit such artifacts, and these phenomena bear on the use of *DOG* operators and the size of the smallest operator proposed by Marr, Poggio and Hildreth [6].

The size of the smallest *DOG* operator in human vision proposed has an excititory center diameter of $1.3'$ [6]. Image features which subtend an angle smaller than $1.3'$ will be subject to swing-wide artifacts due to the smoothing properties of the underlying Gaussian filter [1]. The following figures show the convolution values that would result when viewing the checkerboard near the limit of resolution of the smallest operator. Fig. 1 depicts the input image to the filtering operation. This image consists of a set of computer-generated checkerboard patterns placed in a grey background which is one half the difference of the intensity of black and white squares. The square sizes of the the patterns are 6, 8, 11 and 14

pixels.

A *DOG* operator with a central excitatory diameter (ω) of 11 pixels was used to filter Fig. 1. If the size of this operator is equated to the 1.3′ channel in human vision, the individual squares of Fig. 1 would subtend angles of .71′, .95′, 1.3′, and 1.65′. This operator was balanced such that the overall area integrated to zero, and the skirt was of sufficient length following the specifications of Grimson and Hildreth [3].

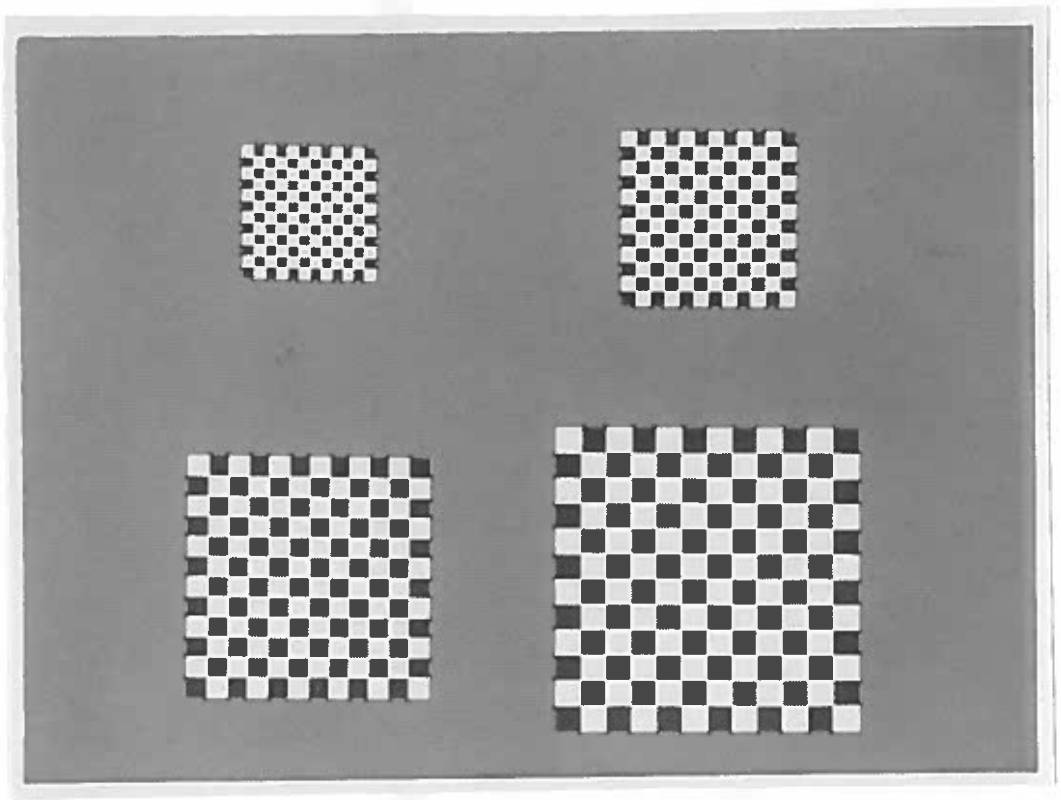

Fig. 1. Checkerboard patterns set in a grey background where the grey is chosen to match the the spatially averaged brightness of the checkerboard. The sizes of individual squares of the patterns are 6, 8, 11, and 14 pixels respectively.

Fig. 2 depicts the raw convolution values in a linear grey scale where white is the highest positive value and black the lowest negative value. This figure clearly shows the smoothing properties of the underlying Gaussian, in particular with checkerboards consisting of squares of 6 and 8 pixels. The border squares are elongated and corner squares are enlarged and rounded. Fig. 3 is a numerical topographic profile of the lower right-hand corner of the convolved values of the checkerboard of 6 pixel squares. The range of values is ± 128. The

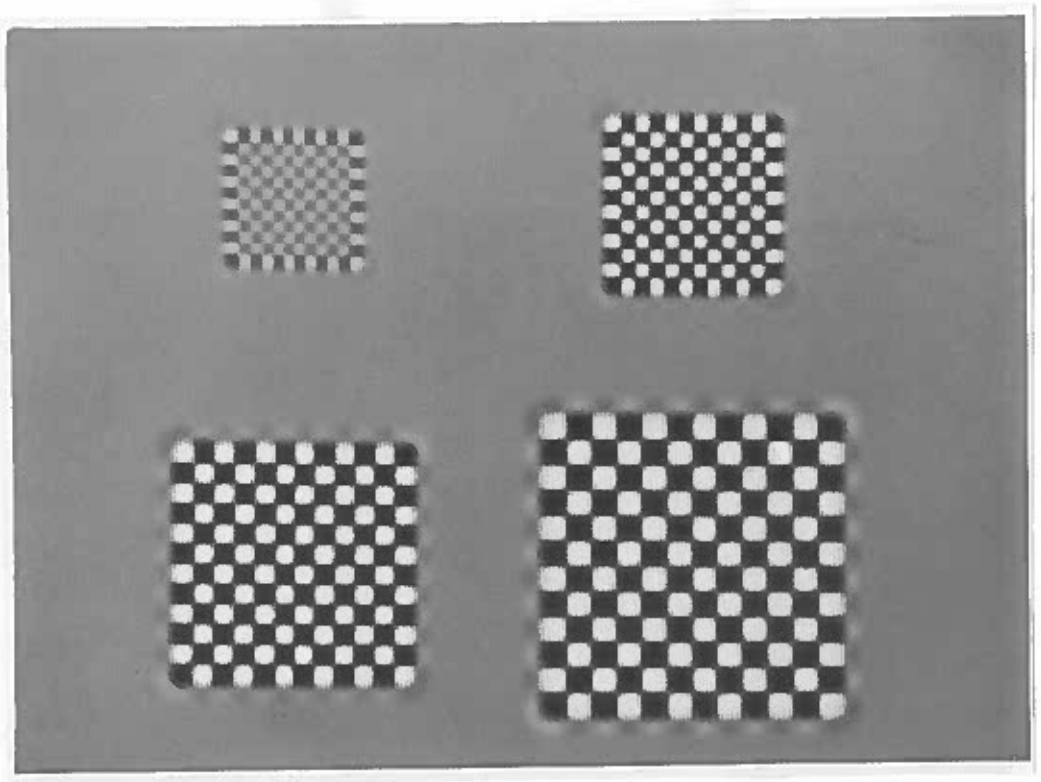

Fig. 2. Raw convolution values are presented in a linear grey scale. Fig. 1. was convolved with an *DOG* operator with a central excitatory diameter of 11 pixels. Notice elongation and rounding of border and corner squares in the top two patterns. In these patterns the square sizes of the original checkerboards are smaller than the diameter of the operator.

elongation and rounding of border and corner squares can be resolved in this figure with a granularity of approximately $7''$ between samples.

9	11	9	5	0	-6	-10	-11	-10	-6	-1	5	10	14	16	16	14	11	9	6	4	2	1	1	0	0	0	0
14	16	14	8	0	-8	-14	-17	-15	-9	0	8	17	23	25	25	22	18	13	9	6	3	2	1	0	0	0	0
15	17	15	8	0	-9	-15	-18	-16	-9	0	10	19	25	28	27	24	20	15	10	7	4	2	1	1	0	0	0
12	14	12	7	0	-7	-12	-14	-12	-7	0	8	15	20	22	22	20	17	13	9	6	4	2	1	1	0	0	0
5	6	5	3	0	-3	-6	-6	-6	-4	0	3	6	9	10	10	10	8	7	5	4	3	2	1	1	0	0	0
-3	-3	-3	-2	0	1	3	3	2	1	-1	-3	-5	-5	-5	-5	-3	-2	0	1	1	2	1	1	1	1	0	0
-9	-11	-9	-5	0	5	9	10	9	4	-2	-8	-14	-17	-19	-17	-15	-11	-7	-4	-1	0	1	1	1	1	0	0
-14	-16	-14	-8	0	8	14	16	13	7	-2	-12	-21	-26	-29	-27	-23	-18	-12	-7	-4	-1	0	0	1	0	0	0
-15	-17	-15	-9	0	8	15	17	14	7	-3	-13	-23	-29	-32	-30	-26	-21	-15	-9	-5	-2	-1	0	0	0	0	0
-12	-14	-12	-7	0	6	11	13	11	5	-3	-12	-20	-25	-27	-26	-23	-18	-13	-8	-5	-2	-1	0	0	0	0	0
-5	-6	-5	-3	0	2	4	5	3	0	-4	-8	-11	-14	-15	-15	-13	-11	-8	-5	-3	-2	-1	-1	0	0	0	0
4	4	4	2	0	-3	-5	-6	-6	-5	-4	-2	-1	0	0	0	-1	-1	-1	-2	-2	-1	-1	-1	-1	0	0	0
11	13	11	6	0	-7	-13	-15	-14	-10	-4	3	9	13	14	13	11	8	5	2	0	-1	-1	-1	-1	-1	0	0
19	21	18	10	0	-11	-20	-23	-21	-14	-4	8	18	24	27	25	21	16	10	5	2	0	-1	-1	-1	-1	-1	0
23	27	23	13	0	-14	-24	-29	-26	-16	-4	10	23	31	35	33	28	21	13	7	3	0	-1	-2	-1	-1	-1	0
25	29	25	14	0	-15	-26	-31	-28	-18	-4	11	24	33	37	35	29	22	14	7	3	0	-2	-2	-2	-1	-1	0
23	27	23	13	0	-14	-24	-29	-26	-17	-4	10	22	30	33	31	26	19	12	6	2	-1	-2	-2	-2	-1	-1	0
20	23	20	11	0	-12	-21	-25	-22	-15	-4	7	17	24	27	25	21	15	9	4	1	-1	-2	-2	-2	-1	-1	0
17	19	17	10	1	-8	-16	-19	-17	-11	-3	6	13	18	20	18	15	10	6	2	-1	-2	-2	-2	-2	-1	-1	0
13	15	13	8	2	-5	-10	-13	-12	-8	-2	4	9	12	13	12	9	6	2	0	-2	-2	-2	-2	-2	-1	-1	0
10	11	10	7	2	-2	-5	-7	-7	-4	-1	2	5	7	7	6	4	2	0	-2	-2	-3	-2	-2	-1	-1	-1	0
7	8	7	5	3	0	-2	-3	-3	-2	0	1	3	3	3	2	1	-1	-2	-2	-3	-2	-2	-2	-1	-1	-1	0
5	5	5	4	2	1	0	-1	-1	0	0	1	1	1	0	0	-1	-2	-2	-3	-2	-2	-2	-1	-1	-1	0	0
3	3	3	3	2	2	1	1	0	0	0	0	0	0	-1	-2	-2	-2	-2	-2	-2	-2	-1	-1	-1	0	0	0
2	2	2	2	2	1	1	1	1	1	0	0	0	-1	-1	-2	-2	-2	-2	-2	-2	-1	-1	-1	-1	0	0	0
1	1	1	1	1	1	1	1	1	1	0	0	0	-1	-1	-1	-2	-2	-2	-1	-1	-1	-1	-1	0	0	0	0
1	1	1	1	1	1	1	1	1	0	0	0	0	-1	-1	-1	-1	-1	-1	-1	-1	-1	0	0	0	0	0	0
0	0	0	0	0	0	0	0	0	0	0	0	0	-1	-1	-1	-1	-1	-1	-1	-1	0	0	0	0	0	0	0
0	0	0	0	0	0	0	0	0	0	0	0	0	0	0	0	0	0	0	0	0	0	0	0	0	0	0	0
0	0	0	0	0	0	0	0	0	0	0	0	0	0	0	0	0	0	0	0	0	0	0	0	0	0	0	0

Fig. 3. A topographic profile of the convolved values from the lower right-hand corner of the smallest pattern in Fig. 2. The positive values are in bold-face and the negative values in italics. Note that the topographic contours follow the elongation and rounding artifacts, and that the values are greater along the border squares.

Fig. 4 displays a binarized version of Fig. 2. All the positive values of the convolution are white and all negative values are black. Notice that the zero-crossings of the convolution "swing wide" of the actual positions of edges along the borders and in the corners, and that these artifacts increase as the squares subtend less than the excitatory diameter ω of the operator. The checkerboard with 6-pixel squares displays zero-crossings which are elongated 2:1 in length vs. width. The zero-crossings of the corner squares bloom such that the zero crossing loci approach a circle of radius 3.45-pixels centered at the most exterior corner of the square in the image. The swing-wide artifacts shown above are consistent with the measurements of Berzins [1].

Figs. 4 and 5 mimic the effect of reducing the scale of the checkerboard. Several phenomena can be seen, including the elongation of the border squares and rounding of the corners squares as they subtend smaller and smaller visual angles, approaching the limits defined by Berzins [1]. In addition, the local energy of the convolution in the interior squares diminishes as the pattern is reduced in scale, since the inhibitory and excitatory regions receive, in the limit, equal energy. The lack of symmetry along the border tends to preserve the edge contrast of these squares, such that for any threshold (either of energy or slope across the zero crossings) the border details are preserved longer than the interior. Note that we chose to balance the background grey to a value intermediate between the white and black squares to enhance this effect. When the interior squares are so small as to no longer be distinguishable from a uniform grey, one can still discern the border of the checkerboard as a thin outline of alternating black and white pinpoints, each rounded and slightly elongated, set against the grey background (see Fig. 5). (If the checkerboard background were white or black instead of grey, the artifacts would still be present and about the same size. A grey background, however, optimizes the contrast of the artifacts at border and corner squares.)

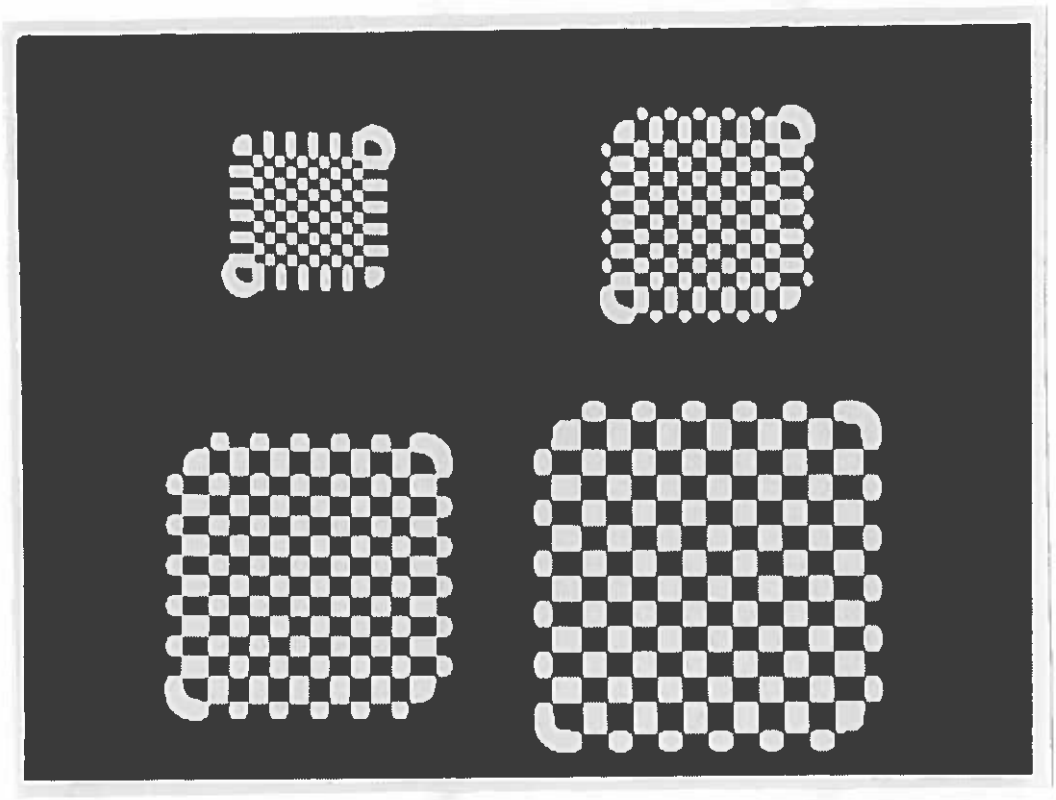

Fig. 4. Binarized version of Fig. 2. Positive values are white and negative values are black. Notice that the zero-crossing contours swing wide of the true edge position along the borders and in the corners. This effect is most extreme in the smallest pattern.

IV. Perceived Artifacts

In order to quantify the original observations a psychophysical experiment was performed. A fine-grain transparency was generated by an Optronix photowriter of a black and white checkerboard pattern on an intermediate grey background. The background grey-level was chosen to match the apparent mean intensity of the checkerboard when the squares can no longer be resolved. The size of the individual squares of the checkerboard was 0.2×0.2

mm. The transparency was back-illuminated with a mean luminance of 7.3 fL. Three skilled observers with excellent vision viewed the pattern at varying distances; all subjects were adapted to normal interior light levels.

The subjects viewed the pattern at increasing distances, marking the distance at which the interior squares vanished, then marking the (somewhat greater) distance at which the borders finally vanished. The subjects also viewed the pattern at decreasing distances

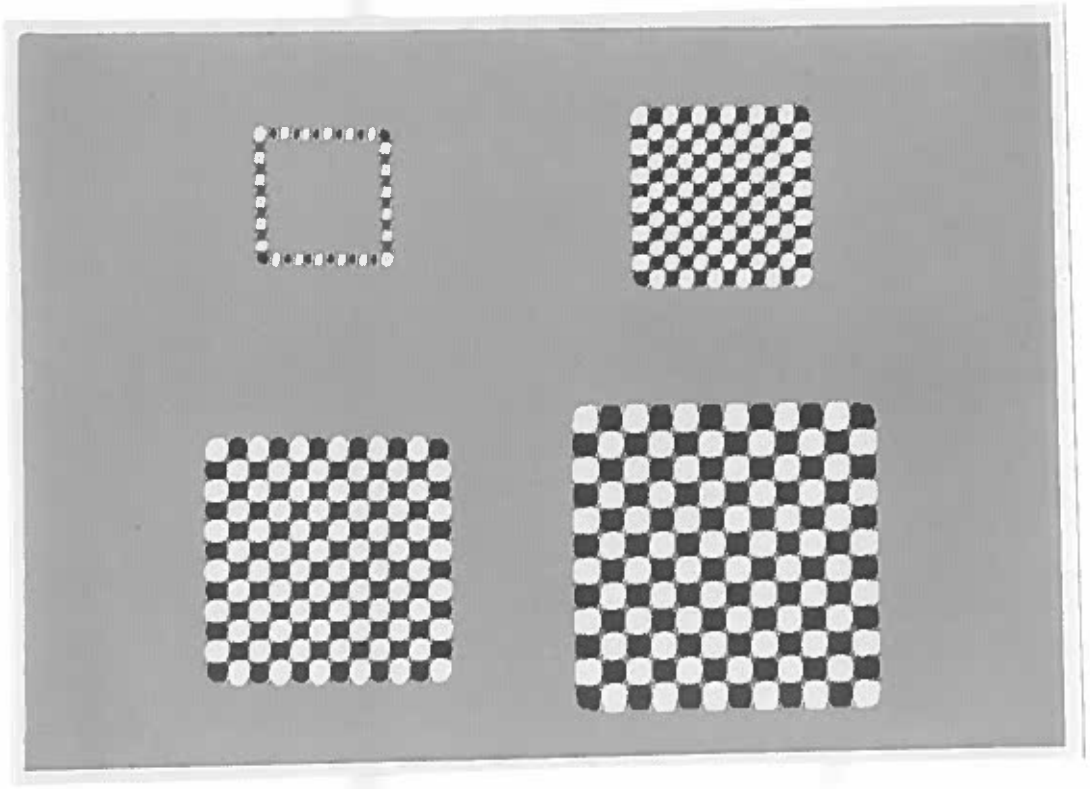

Fig. 5. Thresholded version of Fig. 2. A dead band of ±28 centered at zero is mapped to grey; convolution values of greater positive or negative magnitude are mapped to white or black. Note the increasing border enhancement and eventual extinction of interior detail.

marking the distances where the borders became apparent and the interior could be just discerned. The means of these two distances were determined, from which the corresponding angular subtenses of the squares, in arc minutes, were computed (see table 1).

All observers reported rounded, elongated shapes which corresponded well with the swing-wide artifacts in the zero-crossings that arise when the checkerboards are convolved with DOG operators having ω larger than the square size.

Table 1: Results

subject	interior vanish	borders vanish
1	$1.01'$	$.77'$
2	$1.08'$	$.72'$
3	$1.13'$	$.74'$
Mean	$1.07'$	$.74'$
S.D.	$.06'$	$.03'$

V. Concluding Remarks

The above data suggests that swing-wide artifacts are visible in the perception of intensity events at the limit of human visual resolution. These artifacts are predicted by the filtering properties of the DOG at scales smaller than ω of the operator. The human visual system appears to mimic this behavior. The data was also consistent with the existence of DOG-shaped operators in early visual processing [10, 9].

By looking at the scale at which the artifacts manifest themselves (i.e. between where the interior squares vanish and the border squares vanish), we can estimate the size of the excitatory center of the DOG operator. The data shows that artifacts seen by subjects would be generated by an operator whose size is consistent with the $1.3'$ operator proposed by Marr *et al.* [6].

Since the experiment was conducted at the theoretical and physical limit of resolution, the fact that subjects could still report the shape of the artifacts suggests that a hyperacuity mechanism may be involved. However, such a conclusion is dependent on the representation assumed to underlie the shape judgements. If the shape of intensity changes is carried by the geometry of zero-crossing loci, subjects are seemingly able to resolve zero-crossing details with radii of curvature roughly in the hyperacuity range (the radius of curvature in Fig. 3 is under 20″). But alternatively, if minute intensity changes are described more topographically, e.g. as blobs having elongation and width, these features would be detectable in the normal two-point acuity range (e.g. the smallest elongation is 1.3′ long and .71′ wide).

REFERENCES

[1] Berzins, V., "Accuracy of Laplacian edge detectors," *Computer Vision, Graphics, and Image Processing*, vol. 27, pp. 195-210, 1984.

[2] Enroth-Cugell, C., and Robson, J.D., "The contrast sensitivity of retinal ganglion cells of the cat," *J. Physiol. (Lond.)*, vol. 187, pp. 517-522, 1966.

[3] Grimson, W.E.L., and Hildreth, E., "Comments on "Digital of second directional derivatives"," *IEEE Trans. Pattern Anal. Mach. Intell.*, vol. PAMI-7, no. 1, pp. 121-126, 1985.

[4] Lulich, D.P., "Zero-crossings: symbolic primitives emulating physiologic encoding schemes," M.S. thesis, Oregon Graduate Center., 1985.

[5] Marr, D., and Hildreth, E., "Theory of edge detection," *Proc. Roy. Soc. London*, ser. B, vol. 207, pp. 187-217, 1980.

[6] Marr, D., Poggio, T., and Hildreth E., "Smallest channel in early human vision," *J. Opt. Soc. Am.*, vol. 70, pp. 860-870, 1980.

[7] Torre, V., and Poggio, T.A., "On edge detection," *IEEE Trans. Pattern Anal. Mach. Intell.*, vol. PAMI-8, pp. 147-163, 1986.

[8] Westheimer, G., and McKee, S.P, "Spatial configurations for visual hyperacuity," *Vision Res.*, vol. 17, pp. 941-947, 1977.

[9] Wilson, H.R., and Bergen, J.R., "A four mechanism model for threshold spatial vision," *Vision Res.*, vol. 19, pp. 19-32, 1979.

[10] Wilson, H.R., and Giese, S.A., "Threshold visibility of frequency gradient patterns," *Vision Res.*, vol. 17, pp. 1177-1190, 1977.